

# *Ab-initio* calculations on two-electron ions in strongly coupled plasma environment

S. Bhattacharyya<sup>1,\*</sup>, J. K. Saha<sup>2</sup>, T. K. Mukherjee<sup>3</sup>

<sup>1</sup>*Acharya Prafulla Chandra College, New Barrackpore, Kolkata 700131, India*

<sup>2</sup>*Indian Association for the Cultivation of Science, Jadavpur, Kolkata 700032, India*

<sup>3</sup>*Narula Institute of Technology, Agarpara, Kolkata 700109, India*

\*E-mail : sukhamoy.b@gmail.com

## Abstract

In this work, the controversy between the interpretations of recent measurements on dense aluminum plasma created with Linac coherent light sources (LCLS) X-ray free electron laser (FEL) and Orion laser has been addressed. In both kind of experiments, helium-like and hydrogen-like spectral lines are used for plasma diagnostics. However, there exist no precise theoretical calculations for He-like ions within dense plasma environment. The strong need for an accurate theoretical estimates for spectral properties of He-like ions in strongly coupled plasma environment leads us to perform *ab initio* calculations in the framework of Rayleigh-Ritz variation principle in Hylleraas coordinates where ion-sphere potential is used. An approach to resolve the long-drawn problem of numerical instability for evaluating two-electron integrals with extended basis inside a finite domain is presented here. The present values of electron densities corresponding to disappearance of different spectral lines obtained within the framework of ion-sphere potential show excellent agreement with Orion laser experiments in *Al* plasma and with recent theories. Moreover, this method is extended to predict the critical plasma densities at which the spectral lines of H-like and He-like carbon and argon ions disappear. *Incidental degeneracy* and *level-crossing* phenomena are being reported for the first time for two-electron ions embedded in strongly coupled plasma. Thermodynamic pressure experienced by the ions in their respective ground states inside the ion-spheres are also reported.

## 1 Introduction

The study of confined quantum mechanical systems has attracted immense attention from researchers around the world due to the novel and unusual structural properties exhibited by such systems when subject to spatial limitation [1]. A wide variety of physical situations are manifested in nature that relates to spatially confined systems such as atoms or molecules trapped in zeolite sieves [2], fullerenes [3], plasma environment [4], solvent environment [5], under high pressure in the walls of nuclear reactors [6], quantum dot or artificial atom [7], molecular containers, storage of fuel cells [8,9], matter under high pressure in Zovian planets [10] *etc.* Along with the experimental and technological development, theoretical research plays a fundamental role for designating appropriate models in order to explore and predict the behavioral changes of a confined system. The present study is focused on atomic systems embedded in plasma environment. In recent years, atoms placed in external plasma environment have received considerable attention from researchers [11–19] due to their wide applications in various disciplines of science *e.g.* astrophysics, condensed matter physics, biology *etc.* While dealing with plasma that follows classical statistics, a coupling parameter ( $\Gamma$ ) defined as the ratio of the average electrostatic energy and the average thermal energy is introduced.

$\Gamma < 1$  corresponds to weakly coupled plasma (WCP) for which the effective potential experienced by the embedded ion is expressed according to *Debye* model [20] and  $\Gamma \geq 1$  denotes strongly coupled plasma (SCP) where the potential is taken from Ion-sphere (IS) model [21]. According to the IS model, a sphere (termed as *Wigner-Seitz sphere*) surrounding a positively charged ion is considered in such a way that the plasma electrons within the sphere neutralize the positive ion. The size of the *Wigner-Seitz* sphere will decrease when the number density of plasma electrons ( $n_e$ ) increases. The temperature ( $T$ ) of the plasma does not appear directly in this model but it is implicit as  $n_e$  is different for different temperatures. The domain of the effective potential representing the SCP surrounding is finite in case of IS model in contrast to the long range character of the screened Coulomb potential used in *Debye* model [20] for WCP environment. The examples of WCP's are the gaseous discharge plasma ( $T \sim 10^4$  K and  $n \sim 10^{11}/\text{c.c.}$ ), plasma in controlled thermo-nuclear reaction ( $T \sim 10^8$  K and  $n \sim 10^{16}/\text{c.c.}$ ), solar coronal plasma ( $T \sim 10^6 - 10^8$  K and  $n \sim 10^6 - 10^{10}/\text{c.c.}$ ), Tokamak plasma ( $T \sim 10^5 - 10^7$  K and  $n \sim 10^8 - 10^{16}/\text{c.c.}$ ) etc. SCP's (temperature varies and typical densities  $\geq 10^{23}/\text{c.c.}$ ) are observed in highly evolved stars in high density states, interior of Jovian planets, explosive shock tubes, two-dimensional states of electrons trapped in surface states of liquid helium, laser produced plasmas etc. Spectral line shifts, pressure ionization, ionization potential depression (IPD) and line merging phenomena occur in SCP environment due to the deformation of the ionic potential by the plasma fields. Such properties and knowledge about ion-plasma interaction can effectively be utilized for diagnostics and the investigation of X-ray opacity of matter under conditions prevailing in stellar interiors. The experimental observations using laser produced plasmas for *C*, *Al* and *Ar* by Nantel *et. al.* [22], Saemann *et. al.* [23] and Woolsey *et. al.* [24] have explicitly demonstrated the effect of SCP on the spectral properties of such systems. The laboratory plasma conditions ( $T$  and  $n_e$ ) undergo rapid changes *w.r.t.* where local thermodynamic equilibrium is not maintained. Consequently, the experimental measurements become extremely complicated leading to a loss of accuracy and, till the end of the last century, this accuracy level was not even mentioned in most of the experiments.

In recent years, a remarkable improvement has been made [25–28] with the advent of Linac Coherent Light Sources (LCLS) towards creation of relatively long-lived high-density plasma at homogeneous temperature and densities. In these experiments, X-ray free-electron Laser (FEL) was used to create plasma with densities up to almost one order higher than solid *Al* and then spectral line profiles of different charge states of *Al* were used for diagnostics. The effect of IPD on the emitted spectra as a function of  $n_e$  is explored experimentally by observing the disappearance of spectral lines of H-like and He-like *Al*. During the observation of K-shell fluorescence of highly charged *Al*, Ciricosta *et al.* [27] found that the IPDs measured were not consistent with the predictions of the most widely used theoretical model of Stewart and Pyatt (SP) [29] but in good agreement with an earlier model due to Ecker and Kröll (EK) [30]. However, this observation was questioned in a subsequent theoretical study by Preston *et al.* [31] where detailed simulations were carried out for the spectral lines of H-like and He-like *Al* to study IPD by using both SP and EK (in a modified form) models. In experiments, the intensities and Stark-broadened widths of He- $\beta$  and Ly- $\beta$  spectral lines are used for main diagnostics. A direct measurement of ionization potential depression is a difficult task because of its indistinguishability from the effect of spectral line merging due to Stark broadening [32]. Hoarty *et al.* [33,34] have been able to overcome this difficulty and their measurements for *Al* plasma using Orion laser are in closer agreement with SP model of IPD than the EK model. This situation clearly warrants extensive and accurate *ab initio* study of atomic structures within dense plasma environment. Very recently, Son *et al.* [35] have adopted a two step Hartree-Fock-Slater approach to assess the IPD effect for  $Al^{3+}$  to  $Al^{7+}$  within plasma where a muffin-tin flat potential was used. The IPDs calculated by Son *et al.* [35] lie between the SP and modified EK models and in some cases, are close to SP model. But so far, no extensive theoretical calculation on IPDs for He-like ions has been performed. It should be noted here that both SP model and EK model for estimating

IPDs are derived within the framework of IS potential. The only theoretical work for He-like ions in the field of SCP by using IS potential is due to Sil *et. al.* [36] where both non-relativistic and relativistic calculations were carried out using time-dependent perturbation theory. Though Sil *et. al.* [36] demonstrated that the relativistic IS model yields consistent results in predicting the spectral line positions for the systems considered, some anomalies such as better agreement of non-relativistic results with experiments than relativistic ones are observed in their data [36]. Such strange features may arise due to improper inclusion of electron correlation in basis set within a finite region. A major challenge for precise theoretical calculations is, therefore, to develop an appropriate methodology where the effect of electron correlations within a finite domain is aptly included.

To the best of our knowledge, there exists no calculation of He-like atoms embedded in SCP using Hylleraas type basis set though it is well accepted that within the framework of Ritz variational technique, explicitly correlated wave functions expanded in terms of Hylleraas basis (and its variants) can produce most accurate non-relativistic energies of He-like atoms. These methods have been applied extensively to free He-like systems whereas for spatially confined two-electron systems, such studies are limited to S states only [37–40]. According to Laughlin and Chu [39], the generalized Hylleraas basis sets used in such calculations suffer the loss of linear independence for large dimensions of the wave functions and hence all the calculations [37–40] were limited to small dimensions (at best 25). Laughlin and Chu [39] made an effort to remove this difficulty and extended the basis size up to 95 parameters where they have to compromise with the flexibility of the non-linear parameters. Recently, for  $^1S^e$  states of He-like systems under spherical confinement, the present authors have calculated the energy values [41] by using standard Hylleraas basis set of dimension 161 and the results have been confirmed by Montgomery and Pupyshev [42]. In the present work, a successful effort has been made to develop a general methodology in Hylleraas basis for both  $S$  and  $P$  states of He-like systems. The finite domain two-electron integrals with flexible parameters are evaluated where the problem of linear dependency in larger dimensions is clearly avoided.

We have estimated precise non-relativistic energy values of  $1sns$  ( $^1S^e$ ) [ $n = 1 - 3$ ] and  $1sn'p$  ( $^1P^o$ ) [ $n' = 2 - 4$ ] states of He-like  $C$ ,  $Al$  and  $Ar$  within SCP environment. Accuracy of the computed energy eigenvalues have been tested systematically over an extended range of parameters and also by increasing the number of terms ( $N$ ) in the expanded basis sets. The plasma densities ( $n_e$ ) are varied from a low value that corresponds to almost a free system to a very high one that leads the ion towards destabilization. The plasma electron densities in different experimental conditions [22–28, 33] are well covered within the density ranges studied here. The energy eigenvalues of  $ns$  ( $^2S$ ) [ $n = 1 - 2$ ] and  $n'p$  ( $^2P$ ) [ $n' = 2 - 3$ ] states of H-like  $C$ ,  $Al$  and  $Ar$  in SCP are also estimated to determine the variation of ionization potential (IP) *w.r.t.*  $n_e$ . As  $n_e$  increases, both the two-electron excited states as well as the respective one-electron threshold move towards destabilization, thereby reducing the IP. It is remarkable that after a certain value of  $n_e$ , the two-electron energy levels move above the respective one-electron energy level and become quasi-bound. *Incidental degeneracy* [43] and subsequent *level-crossing* phenomenon between the excited states such as  $1s2s$  ( $^1S^e$ ) and  $1s2p$  ( $^1P^o$ ) under SCP have been observed. Such features are novel in the context of foreign atoms in SCP and being reported for the first time in literature. Due to spatial restriction imposed upon the wave function according to IS model under SCP environment, the ion will feel a pressure inside the *Wigner-Seitz* sphere. The variation of thermodynamic pressure *w.r.t.* plasma density is also calculated. The paper is organized as: an outline of the basic theory used and details on the evaluation of the basis integrals are given in Section 2, followed by a discussion on the results in Section 3 and finally concluded in section 4 with a view towards further application of the present methodology in related fields.

## 2 Method

The non-relativistic Hamiltonian (in a.u.) of a two-electron ion placed inside SCP environment can be written as

$$H = \sum_{i=1}^2 \left[ -\frac{1}{2} \nabla_i^2 + V_{IS}(r_i) \right] + \frac{1}{r_{12}} \quad (1)$$

$V_{IS}(r_i)$  is the one-electron term of the modified potential energy as ‘seen’ by the  $i$ -th electron within plasma environment. It is to be noted that in this model, the electronic repulsion part in the potential is completely unaltered. The spherically symmetric potential  $V_{IS}(r_i)$  experienced by a positive charge ion surrounded by a one-component plasma within the ion-sphere [21] is given by

$$V_{IS}(r_i) = -\frac{Z}{r_i} + \frac{(Z - N_e)}{2R} \left[ 3 - \left( \frac{r_i}{R} \right)^2 \right] \quad (2)$$

where  $R$  is the *Wigner-Seitz* radius [21], *i.e.* the radius of the surrounding ion-sphere,  $Z$  is the nuclear charge and  $N_e$  ( $< Z$ ) is the number of electrons present in the ion. For helium-like ions,  $N_e = 2$  is being taken. The Schrodinger equation  $H\Psi = E\Psi$  is to be solved to obtain the energy eigenvalues where the wave function is subject to the normalization condition  $\langle \Psi | \Psi \rangle = 1$  within the sphere. The structure of the potential demands that there is no electron current taking place through the boundary surface of *Wigner-Seitz* sphere, and the orbital wave function  $\Psi$  satisfies the boundary condition

$$\Psi(r) = 0 \quad \text{at } r \geq R \quad (3)$$

This boundary condition plays a significant role in behavioral changes of the confined atoms. The plasma electrons within the ion-sphere neutralize the central positive charge and the size of the *Wigner-Seitz* sphere is determined by the condition of overall charge neutrality that yields

$$R = \left[ \frac{3(Z - N_e)}{4\pi n_e} \right]^{\frac{1}{3}} \quad (4)$$

The above expression for ‘ $R$ ’ is used to determine the IPD according to the SP model [29]. However, in EK model [30] for determining the IPD, this radius was calculated in a somewhat different way where both the electron density ( $n_e$ ) and ion density ( $n_i$ ) are considered. According to EK model [30], the radius of the sphere would be expressed as

$$R_{EK} = \left[ \frac{3}{4\pi(n_e + n_i)} \right]^{\frac{1}{3}} \quad (5)$$

The EK model [30] is relevant when the ion density is appreciably high and can affect the mean separation of the free electrons.

Due to the translational symmetry of the Hamiltonian of a two-electron ion, the degrees of freedom reduce from nine to six by separating the motion of the centre of mass. These six coordinates can be taken as the sides of the triangle  $r_1, r_2, r_{12}$  formed by the three particles, *i.e.*, two electrons and the fixed nucleus and the Eulerian angles  $(\theta, \phi, \psi)$  defining the orientation of this triangle in space. The wave function obeying symmetry properties under particle exchange may be written as [44]

$$\Psi(\vec{r}_1, \vec{r}_2) = \sum_{\kappa} [f_L^{\kappa+}(r_1, r_2, \theta_{12}) D_L^{\kappa+}(\theta, \phi, \psi) + f_L^{\kappa-}(r_1, r_2, \theta_{12}) D_L^{\kappa-}(\theta, \phi, \psi)] \quad (6)$$

$\theta_{12}$  is the angle between  $\vec{r}_1$  and  $\vec{r}_2$ . The summation in eq. (6) goes over every alternate value of  $\kappa$ , where  $\kappa = |k|$ .  $k$  is the angular momentum quantum number about the body fixed axis of rotation whose value satisfies  $k \leq L$ ,  $L$  being the total angular momentum quantum number. The symmetric top functions  $D_L^{\kappa+}$  and  $D_L^{\kappa-}$  are the eigenfunctions of angular momentum operator  $L^2$  of the two electrons. The rotational invariance of the Hamiltonian makes it possible to express the variational equation of two electrons in the field of a fixed nucleus in terms of three independent variables  $r_1$ ,  $r_2$  and  $r_{12}$  (or  $\theta_{12}$ ). The reduction of the Eulerian angles from the variational equation is an immediate consequence of the spherical symmetry of the field.

### For $^1S^e$ state

The variational equation for  $^1S^e$  states originating from two s-electrons (1sns configuration) is given by, following ref. [45],

$$\delta \int \left[ \frac{1}{2} \left( \frac{d\Psi_S}{dr_1} \right)^2 + \frac{1}{2} \left( \frac{d\Psi_S}{dr_2} \right)^2 + \left( \frac{r_1^2 - r_2^2 + r_{12}^2}{2r_1r_{12}} \right) \left( \frac{d\Psi_S}{dr_1} \right) \left( \frac{d\Psi_S}{dr_{12}} \right) + \left( \frac{r_2^2 - r_1^2 + r_{12}^2}{2r_2r_{12}} \right) \left( \frac{d\Psi_S}{dr_2} \right) \left( \frac{d\Psi_S}{dr_{12}} \right) + (V - E)\Psi_S^2 \right] dV_{r_1, r_2, r_{12}} = 0 \quad (7)$$

where the upper limit of integration for  $r_1$  and  $r_2$  is  $R$  in contrast to infinity for the free atomic case. The upper and lower limits of integration for  $r_{12}$  are  $(r_1 + r_2)$  and  $|r_1 - r_2|$ , respectively. The volume element is expressed as

$$dV_{r_1, r_2, r_{12}} = r_1 r_2 r_{12} dr_1 dr_2 dr_{12} \quad (8)$$

For  $S$ -states,  $L = \kappa = 0$  and the wave function  $\Psi_S$  can be written as

$$\Psi_S = f_0^0 D_0^0 = f_S + \tilde{f}_S \quad (9)$$

where  $\tilde{f}_S(r_1, r_2, r_{12}) = f_S(r_2, r_1, r_{12})$ . The correlated wave function [41] is written as

$$f_S(r_1, r_2, r_{12}) = (R - r_1)(R - r_2)f(r_1, r_2, r_{12}) \quad (10)$$

with

$$f(r_1, r_2, r_{12}) = e^{-\sigma_1 r_1 - \sigma_2 r_2} \sum_{l \geq 0} \sum_{m \geq 0} \sum_{n \geq 0} C_{lmn} r_1^l r_2^m r_{12}^n \quad (11)$$

$\sigma_1$  and  $\sigma_2$  are the nonlinear parameters taking care of the effect of radial correlation in the wave function whereas the angular correlation effect is incorporated through different powers of  $r_{12}$ .  $C$ 's are the linear variational parameters. The total number of parameters ( $N$ ) in the basis set is defined as the total number of different  $(l, m, n)$  sets (eq. 11) taken in the expansion of  $f(r_1, r_2, r_{12})$ .

### For $^1P^o$ state

For  $P$  state of odd parity ( $L = 1$  and  $\kappa = +1, -1$ ), the total wave function can be written as [46]

$$\Psi_P = f_1^{1+} D_1^{1+} + f_1^{1-} D_1^{1-} \quad (12)$$

The origin of  $^1P^o$  state due to  $sp$  configuration of two-electron atoms can be shown by expressing  $D_1^{1+}$  in terms of individual polar coordinates  $(\theta_1, \phi_1; \theta_2, \phi_2)$  as given below:

$$D_1^{1+}(\theta, \phi, \psi) \cos \frac{\theta_{12}}{2} = P_0^0(\cos \theta_1) P_1^0(\cos \theta_2) + \textit{interchange} \quad (13)$$

Similar expressions for  $D_1^{1-}$  can be derived. After integration over the Eulerian angles, the variational equation for  $^1P^o$  states originating from  $1snp$  configuration reduces to [46],

$$\begin{aligned} \delta \int \left[ \sum_{i=1}^2 \left\{ \left( \frac{\partial f_1^{1+}}{\partial r_i} \right)^2 + \left( \frac{\partial f_1^{1-}}{\partial r_i} \right)^2 \right\} + \left( \frac{1}{r_1^2} + \frac{1}{r_2^2} \right) \left\{ \left( \frac{\partial f_1^{1+}}{\partial \theta_{12}} \right)^2 + \left( \frac{\partial f_1^{1-}}{\partial \theta_{12}} \right)^2 + \left( \frac{1}{4} + \frac{1}{2 \sin^2 \theta_{12}} \right) \times \right. \right. \\ \left. \left\{ (f_1^{1+})^2 + (f_1^{1-})^2 \right\} + \frac{\cos \theta_{12}}{2 \sin^2 \theta_{12}} \left\{ (f_1^{1+})^2 - (f_1^{1-})^2 \right\} \right] + \left( \frac{1}{r_2^2} - \frac{1}{r_1^2} \right) \left\{ \left( \frac{\partial f_1^{1+}}{\partial \theta_{12}} f_1^{1-} - \frac{\partial f_1^{1-}}{\partial \theta_{12}} f_1^{1+} \right) \right. \\ \left. - \frac{1}{\sin \theta_{12}} f_1^{1+} f_1^{1-} \right\} + 2(V - E) \left\{ (f_1^{1+})^2 + (f_1^{1-})^2 \right\} \right] dV_{r_1, r_2, \theta_{12}} = 0 \end{aligned} \quad (14)$$

The correlated functions  $f_1^{1+}$  and  $f_1^{1-}$  can be written as

$$f_1^{1+} = (f_P + \tilde{f}_P) \cos \frac{\theta_{12}}{2} \quad (15)$$

$$f_1^{1-} = (f_P - \tilde{f}_P) \sin \frac{\theta_{12}}{2} \quad (16)$$

where

$$f_P(r_1, r_2, r_{12}) = (R - r_1)(R - r_2)g(r_1, r_2, r_{12}) \quad (17)$$

and

$$g(r_1, r_2, r_{12}) = e^{-\rho_1 r_1 - \rho_2 r_2} \sum_{l \geq 1} \sum_{m \geq 0} \sum_{n \geq 0} D_{lmn} r_1^l r_2^m r_{12}^n \quad (18)$$

The nonlinear parameters *i.e.*  $\sigma$ 's in eq. (11) and  $\rho$ 's in eq. (18) for  $S$  and  $P$  states respectively are optimized separately using Nelder-Mead algorithm [47]. The linear variational parameters *i.e.*  $C_{lmn}$ 's and  $D_{lmn}$ 's along with the energy eigenvalues are obtained by solving the generalized eigenvalue equation

$$\underline{\underline{H}} \underline{\underline{C}} = E \underline{\underline{S}} \underline{\underline{C}} \quad (19)$$

where  $\underline{\underline{H}}$  is the Hamiltonian matrix,  $\underline{\underline{S}}$  is the overlap matrix,  $\underline{\underline{C}}$  is the column matrix consisting of linear variational parameters and  $E$  is the corresponding energy eigenvalue. The wave function is normalized for each confining radius  $R$  to account for the reorientation of charge distribution within the *Wigner-Seitz* sphere. All computations are carried out in quadruple precision to ensure better numerical stability for extended Hylleraas basis sets within a finite domain.

The variational equation for  $nl$  ( $^2L$ ) states of one electron ion within ion-sphere of radius  $R$  can be written as

$$\delta \int_0^R \left[ \frac{1}{2} \left\{ \left( \frac{\partial f}{\partial r} \right)^2 + \frac{l(l+1)}{r^2} f^2 \right\} + \{V_{IS}(r) - E\} f^2 \right] r^2 dr = 0 \quad (20)$$

where, the one-particle effective potential  $V_{IS}(r)$  is taken from eq. (2) with  $N_e = 1$ . The radial function  $f(r)$  is given by

$$f(r) = (R - r)r^k \sum_i C_i e^{-\rho_i r} \quad (21)$$

where  $k = 0$  and  $1$  for  ${}^2S$  and  ${}^2P$  states respectively. In this calculation, we have taken 21 different nonlinear parameters ( $\rho_i$ 's) in a geometrical sequence  $\rho_i = \rho_{i-1}\gamma$ ,  $\gamma$  being the geometrical ratio [13, 48]. Such choice of non-linear parameters enable us to cover the full region of space in a flexible manner by adjusting  $\gamma$ . The energy values  $E$ 's and linear co-efficients  $C_i$ 's are determined from eq. (19).

The truncation of wavefunction at a finite distance (eq. 3) imposes a thermodynamic pressure upon the ions which increases with increase of  $n_e$  inside the sphere. We have calculated the pressure felt by all the hydrogen-like and helium-like ions in their respective ground state using the first law of thermodynamics. However, for excited states having finite lifetime, this approach is not valid as the equilibrium criteria is not maintained. Under an adiabatic approximation, the pressure on the ions in the ground state can be expressed as [41]

$$P = -\frac{1}{4\pi R^2} \frac{dE}{dR} \quad (22)$$

### Evaluation of two-electron integrals

The correlated two-electron basis integrals arising in the present calculations are of the form

$$\begin{aligned} A(a, b, c; \alpha, \beta; R) &= \int_0^R r_1^a e^{-\alpha r_1} \int_0^R r_2^b e^{-\beta r_2} \int_{|r_1-r_2|}^{r_1+r_2} r_{12}^c dr_1 dr_2 dr_{12} \\ &= \int_0^R r_1^a e^{-\alpha r_1} \int_0^{r_1} r_2^b e^{-\beta r_2} \int_{r_1-r_2}^{r_1+r_2} r_{12}^c dr_1 dr_2 dr_{12} + \int_0^R r_2^b e^{-\beta r_2} \int_0^{r_2} r_1^a e^{-\alpha r_1} \int_{r_2-r_1}^{r_1+r_2} r_{12}^c dr_1 dr_2 dr_{12} \end{aligned} \quad (23)$$

For  $S$  states,  $a \geq 0, b \geq 0, c \geq 0$  while for higher angular momentum states ( $P, D$  etc.), integrals with  $a = -1$  also arises. After integration, the  $r_{12}$  part of eq. (23) can be expanded as

$$\frac{1}{n+1} [(r_1 + r_1)^{n+1} - (r_1 - r_1)^{n+1}] = \sum_{i=0}^{\frac{n}{2}} \frac{2 \cdot n!}{(2i+1)!(n-2i)!} r_1^{n-2i} r_2^{2i+1} \quad [n \text{ even}] \quad (24)$$

For odd ' $n$ ', the upper limit of the sum in the right hand side would be replaced by  $\frac{n-1}{2}$ . The integrals from eq. (23) then reduce to the form

$$\int_0^y x^k e^{-\lambda x} dx = \int_0^\infty x^k e^{-\lambda x} dx - \int_y^\infty x^k e^{-\lambda x} dx = \frac{k!}{\lambda^{k+1}} \left[ 1 - e^{-\lambda y} \sum_{j=0}^k \frac{y^j \lambda^j}{j!} \right] \quad (25)$$

$\lambda$  is a positive real number and  $k$  is a non-negative integer and we have used the standard integral

$$\int_0^\infty x^k e^{-\lambda x} dx = \frac{k!}{\lambda^{k+1}} \quad (26)$$

The integral  $A(a, b, c; \alpha, \beta; R)$  is now evaluated for two different cases.

### Case I: $a \geq 0, b \geq 0, c \geq 0$

An exact analytical expression for  $A(a, b, c; \alpha, \beta; R)$  corresponding to  $a \geq 0, b \geq 0, c \geq 0$  has been derived in a straightforward way using eq. (25) and the numerical values are displayed in table-1. In the first column of table-1, different powers of  $r_1, r_2$  and  $r_{12}$  i.e.  $a, b$  and  $c$  are given. For each set of  $(a, b, c)$ , the non-linear parameters  $(\alpha, \beta)$  given in the second column of table-1 are varied from

very low to high values as obtained from the optimized values corresponding to different cases in the present work. The values of  $R$  varied in a wide range for each set of  $(a, b, c)$  and  $(\alpha, \beta)$  are given in the fourth column of table-1. All the values of integrals are given in the in the last column of table-1. We have checked the results with standard mathematical software (*e.g. Maple*) to ensure the numerical stability of the expression for  $A(a, b, c; \alpha, \beta; R)$  over the complete range of  $R$ .

## Case II: $a = -1, b \geq 0, c \geq 0$

After full expansion of the integral  $A(-1, b, c; \alpha, \beta; R)$  over  $r_{12}$  and  $r_2$  by using eqs. (24) and (25) an integral  $I(\alpha, \beta; R)$  arise which takes the form

$$I(\alpha, \beta; R) = \int_0^R \frac{e^{-\alpha r_1} - e^{-(\alpha+\beta)r_1}}{r_1} dr_1 \quad (27)$$

The above integral  $I(\alpha, \beta; R)$  is actually a converging infinite series with oscillatory terms. We have tested the evaluation of the term  $I(\alpha, \beta; R)$  in two different approaches.

i) We can expand the exponential functions to evaluate the integral as

$$\begin{aligned} \int_0^R \frac{e^{-\alpha r_1} - e^{-(\alpha+\beta)r_1}}{r_1} dr_1 &= \sum_{q=0}^{\infty} \int_0^R \frac{1}{r_1} \left[ \frac{(-1)^q}{q!} \{ \alpha^q - (\alpha + \beta)^q \} r_1^q \right] dr_1 \\ &= \sum_{q=1}^{\infty} \frac{(-1)^q R^q}{q \cdot q!} [\alpha^q - (\alpha + \beta)^q] \end{aligned} \quad (28)$$

The expression (28) gives accurate value of integrals where the upper limit  $R$  is small, but fails to produce results when  $R$  is sufficiently high.

ii) Alternatively, the integral  $I(\alpha, \beta; R)$  may be written as

$$\int_0^R \frac{e^{-\alpha r_1} - e^{-(\alpha+\beta)r_1}}{r_1} dr_1 = \int_0^R \frac{e^{-\alpha r_1}}{r_1} (1 - e^{-\beta r_1}) dr_1 = \sum_{q=1}^{\infty} \frac{(-1)^{q-1} \beta^q}{q!} \int_0^R r_1^{q-1} e^{-\alpha r_1} dr_1 \quad (29)$$

The  $r_1$ -integral in the *r.h.s* of equation (29) is then evaluated using expression (25).

The integral  $I(\alpha, \beta; R)$  is calculated by using both the expressions given in eq. (28) and eq. (29). All the results corresponding to different sets of  $(\alpha, \beta; R)$  are given in table 2 which shows excellent agreement among the results except for some high values of  $R$  used in eq. (28). On the other hand, eq. (29) yields excellent results irrespective of the values of the parameters  $(\alpha, \beta)$  over the complete range of  $R$ . In eq. (28), a term  $R^q$  appears in the numerator that increases with increase in  $q$ . For low values of  $R$ , this term is balanced by  $q!$  in the denominator but for high  $R$ , a numerical instability appears because within the first few terms,  $R^q$  bounces more rapidly than  $q!$ . In contrast, a term  $\frac{R^q}{j!} e^{-\alpha R}$  appears in eq. (29) [after expanding the  $r_1$ -integral according to eq. (25)] which falls rapidly as  $q$  increases due to the presence of the exponential term. To have a better understanding of the integrals, we have also checked the convergence of  $I(\alpha, \beta; R)$  evaluated using eqs. (28) and (29) by increasing the number of terms in the infinite series and displayed the convergence behaviour in table 3 for  $R = 100.0$  and  $0.2$  and two sets of  $(\alpha, \beta)$ . It appears from table 3 that for  $R = 100.0$  the values derived from eq. (28) are clearly not acceptable but for low  $R$ , the final results match exactly though the convergence is slow for equation (28). We have finally used eq. (29) to calculate the energy eigenvalues in the present work and taken 1000 terms in the corresponding infinite series to ensure the desired level of accuracy. In table 4 we have given the values of integral  $A(-1, b, c; \alpha, \beta; R)$  corresponding to different sets of parameters. We have further observed that the integrals [eq. (29)] corresponding to  $R = 100$  yield same result as obtained by using eq. (26) for  $R = \infty$ . This is mention further that all the integrals are checked with standard mathematical software.

### 3 Results and discussions

The energy eigenvalues of He-like  $C$ ,  $Al$  and  $Ar$  in  $1sns$  ( $^1S^e$ ) [ $n = 1 - 3$ ] and  $1sn'p$  ( $^1P^o$ ) [ $n' = 2 - 4$ ] states have been calculated within SCP environment using the IS potential. We have studied the convergence of the energy values *w.r.t.* the number of terms ( $N$ ) in the wave function. Table 5 shows the convergence behaviour of  $C^{4+}$  in  $1s^2$  ( $^1S^e$ ) state for some selected values of  $R$ . We have obtained a similar convergence pattern for all the other ions and also for the excited states under consideration. The size of the basis has been extended systematically to  $N = 161$  and  $149$  for  $^1S^e$  and  $^1P^o$  states respectively with  $l + m + n = 10$  [eqs. (11) and (18)]. The convergence of the energy values are obtained at least up to the sixth significant digits. In fact, for some cases *e.g.*  $1s^2$  ( $^1S^e$ ) state of  $C^{4+}$  with  $R = 0.47$  a.u., we have obtained convergence of energy values up to the eighth decimal place, as is evident from table 5. The above observation ensures that the present method can deal with extended basis sets to yield sufficiently accurate energy values within a finite limit.

The energy values of He-like  $C$ ,  $Al$  and  $Ar$  in  $1sns$  ( $^1S^e$ ) [ $n = 1 - 3$ ] and  $1sn'p$  ( $^1P^o$ ) [ $n' = 2 - 4$ ] states within ion-sphere of different radii ( $R$ ) are displayed in tables 6, 7 and 8 respectively. We have also listed the energies of respective H-like ions in  $ns$  ( $^2S$ ) [ $n = 1 - 2$ ] and  $n'p$  ( $^2P$ ) [ $n' = 2 - 3$ ] states. It is worthwhile to mention that under one-component plasma approximation, the IS radius for a two-electron ion would differ from that for a one-electron ion corresponding to the same plasma electron density. We see that as  $n_e$  increases, the energy levels move towards continuum which is a clear manifestation of the positive nature of IS potential. To check the overall behavior of the results, we have plotted the energy values ( $-E$ ) of bound  $1sns$  ( $^1S^e$ ) [ $n = 1 - 3$ ] and  $1sn'p$  ( $^1P^o$ ) [ $n' = 2 - 4$ ] states of  $C^{4+}$  with respect to IS radius ( $R$ ) in figure 1. It is evident from figure 1 that the energy values remain almost unaltered for a range of  $R$  and after that rapidly approaches towards the destabilization limit. Hence the variation produces a ‘*knee*’ around some particular value of  $R$ . For higher excited states, this ‘*knee*’ appears at a higher value of  $R$ . All other ions also show same features. Similar behaviour of energy values of He-like ions inside a spherical impenetrable box (referred to as ‘Coulombic sphere’ hereinafter) was reported in a recent publication [41] where the potential inside the box was purely Coulombic. Within the ion-sphere, energy value of the positively charged ion is modified for two factors:

1. The environment envisaged by IS potential which is governed by plasma electron density *and*
2. The truncation of wave function at a finite distance that generates a pressure on the system.

In order to assess the effect each factor on the energy eigenvalues, we have also studied separately the modification of energy values of two-electron ions due to the truncation of the wave function at different radii of Coulombic sphere. The ground state energy of a ‘*free*’  $C^{4+}$  ion where the wave function is infinitely extended is  $-32.406247$  a.u. whereas within a Coulombic sphere and ion-sphere both having a radius of  $20.0$  a.u., the energy values are  $-32.406247$  and  $-31.806294$  a.u. respectively. It shows that for a large box radius, almost 100% of the shift in the energy is due to the effect of plasma. The truncation of wave function becomes significant when the size of the sphere is reduced. At a radius of  $0.7$  a.u., the ground state energy values of  $C^{4+}$  ion within Coulombic sphere and ion-sphere are  $-31.192275$  and  $-14.880628$  a.u. respectively which shows an effect of almost 7% on the shift of energy level is coming from the truncation of wave function. This effect increases to 22.4% and 26.2% for truncation radius of  $0.5$  and  $0.4692$  a.u. respectively.

A closer look at the results quoted in tables 6 – 8 leads us further to the following observations.

1. **Decrease in number of excited states:** For two-electron ions  $C^{4+}$ ,  $Al^{11+}$  and  $Ar^{16+}$  we see that as  $n_e$  increases, the ions become less bound and also the number of excited states decreases. For example,  $C^{4+}$  exists in the ground state up to  $R = 0.4692$  a.u. but  $1s2s$  ( $^1S^e$ ) state ceases to exist after  $R = 0.9017$  a.u. and  $1s3s$  ( $^1S^e$ ) destabilizes after  $R = 1.3761$  a.u.

Similar feature is observed for all the ions and also for  $^1P^o$  states. For H-like ions of  $C$ ,  $Al$  and  $Ar$ , the  $2s$  state destabilizes much before  $1s$  with increase of  $R$ .

2. **Reduction of ionization potential:** Ionization potential for a two-electron ion is defined as the amount of energy required to ionize one electron from the ground state ( $1s^2$ ). It is observed from tables 6 – 8 for all the ions that with increase in plasma density, IP decreases and beyond certain density, the two-electron energy levels move above the one-electron threshold. We have studied the variation of IPD of two-electron ions *w.r.t.*  $n_e$  from the difference of IP within and without (*i.e.* free case) the surrounding plasma environment. In figure-2, we have plotted the IP and IPD for  $Al^{11+}$  as a function of plasma electron density. The energy required to ionize the outer electron from  $1s3p(^1P^o)$  state *i.e.* IP for  $1s3p(^1P^o)$  state of  $Al^{11+}$  and the corresponding IPD *w.r.t.*  $n_e$  are also included in figure-2. The effect of surrounding plasma on different two-electron energy levels should be different and consequently, IPDs should differ from one configuration to another. It is evident from figure-2 that the present observation corroborates this fact. The two-electron  $^1P^o$  states would give rise to spectral lines via dipole transition until they merge into the one-electron continuum. For example, table-7 shows that  $1s3p(^1P^o)$  state of  $Al^{11+}$  can survive up to the density of  $8.11 \times 10^{25}/c.c.$  whereas it crosses the corresponding  $1s$  threshold after the density of  $2.11 \times 10^{24}/c.c.$  and consequently, the  $He_\beta$  line originating from  $1s3p(^1P^o) \rightarrow 1s^2(^1S^e)$  emission is not expected to be observed after this density. In table 9, we have listed the critical electron densities after which different spectral lines of H-like and He-like  $Al$  disappear. The densities are calculated from IS radius according to both SP model and EK model of determining IPDs following eq. (4) and (5) respectively. For  $Ly_\beta$  line of  $Al^{12+}$  and  $He_\beta$  line of  $Al^{11+}$ , the present electron densities calculated by using SP model are in good agreement with experimental observation [33]. For disappearance of  $He_\gamma$  line, the only theoretical calculation of plasma density is due to Preston *et al.* [31] where a possible range of densities is given. No experimental result is available for comparison in this context. Our results obtained by using SP model of IPD indicate that the  $He_\gamma$  line of  $Al^{11+}$  would disappear after a plasma density of  $5.0 \times 10^{23}/c.c.$ , as is given in table-9. We mention that the disappearance of both  $Ly_\beta$  and  $He_\beta$  lines are experimentally observed at the density of  $2.2 \times 10^{24}/c.c.$  whereas the  $Ly_\beta$  line should survive more than the  $He_\beta$  line. Present results along with ref. [35] as depicted in table-9 establish the fact explicitly. A more accurate experimental measurement is therefore necessary for proper plasma diagnostics. In an earlier experiment, Nantel *et al.* [22] observed  $He_\alpha$ ,  $He_\beta$  and  $He_\gamma$  lines of  $C^{4+}$  at plasma density  $1.5 \times 10^{21}/c.c.$  In this experiment the densities corresponding to disappearance of such He-like lines are not explored. However, table-9 shows that He-like lines of  $C^{4+}$  vanish well above the density of  $1.5 \times 10^{21}/c.c.$  Hence, the existence of such He-like lines of  $C^{4+}$  at the density  $1.5 \times 10^{21}/c.c.$  as observed by Nantel *et al.* [22] are consistent with present calculations. Similar comparisons have been done with other earlier experiments of Saemann *et al.* [23] and Woolsey *et al.* [24] for spectral lines of  $Al^{11+}$  and  $Ar^{16+}$  respectively and the present results are in agreement with the experiments. Accurate measurement like the Orion laser experiment [33] is necessary to confirm the present theoretical predictions for disappearance of spectral lines of  $C^{4+}$  and  $Ar^{16+}$ .
3. **Quasi-bound states of two-electron ions:** Quasi-bound states or continuum bound states may be found in continuous part of the spectra for electronic confinement under different potentials [49] and has also been observed experimentally [50]. These states have great structural similarity with the discrete energy levels. For a two-electron ion, the ground state and all singly excited energy levels, in general, lie below the first ionization threshold. Tables 6-8 show that for high values ‘ $R$ ’ (*i.e.* almost free case), this feature is maintained for all the ions but as  $R$  decreases, all singly excited states of two-electron ions become less bound more rapidly than the respective one-electron ion. For example, at  $R = 20.0$  a.u. the energy values of  $C^{4+}$  as

reported in table-6 lie below the  $1s$  threshold of  $C^{5+}$ . At  $R = 5.0$  a.u. the  $1s4p$  ( $^1P^o$ ) state moves above the  $1s$  threshold but lies below  $2s$  threshold. Similarly, at  $R = 2.0$  a.u.  $1s3s$  ( $^1S^e$ ) and  $1s3p$  ( $^1P^o$ ) states lie above the  $1s$  threshold and below  $2s$  threshold. At  $R < 1.7$  a.u. the  $2s$  level of  $C^{5+}$  destabilizes and we observe well-converged (up to 7th significant digits) energy level of  $1s4p$  ( $^1P^o$ ) state of  $C^{4+}$  embedded in one-electron continuum. Similar feature is obtained for other ions also and is being reported for the first time in SCP.

4. **Incidental degeneracy and level crossing:** For a free two-electron ion, the energy value of  $1s2s$  ( $^1S^e$ ) state is more negative than  $1s2p$  ( $^1P^o$ ) state. Tables 6-8 establish this fact for high values of  $R$  corresponding to all the two-electron ions. For example, the  $1s2s$  ( $^1S^e$ ) level of  $C^{4+}$  lies below  $1s2p$  ( $^1P^o$ ) level for IS radius up to  $R = 2.0$  a.u. At  $R = 1.5$  a.u., the  $1s2s$  ( $^1S^e$ ) state moves above the  $1s2p$  ( $^1P^o$ ) level. These results show that an ‘*incidental degeneracy*’ [43] has taken place for  $1s2s$  ( $^1S^e$ ) and  $1s2p$  ( $^1P^o$ ) states of  $C^{4+}$  at some value of  $R$  between 1.5 and 2.0. a.u. and then a ‘*level crossing*’ occurs between two states having different symmetry properties. The phenomenon of *incidental degeneracy* was reported in case of shell-confined hydrogen atom by Sen [43] where two initially non-degenerate states are brought to a same energy level by adjusting external parameters. For a two-electron ion, we report *incidental degeneracy* for the first time within SCP environment. After the *level crossing*, the  $1s2s$  ( $^1S^e$ ) state of  $C^{4+}$  destabilizes (at  $R = 0.9017$  a.u.) much before  $1s2p$  ( $^1P^o$ ) state (at  $R = 0.797$  a.u.). Similarly, for  $1s3s$  ( $^1S^e$ ) and  $1s3p$  ( $^1P^o$ ) states of  $C^{4+}$ , *incidental degeneracy* and subsequent *level crossing* are observed at a value of  $R$  lying somewhere between 5.0 and 3.0 a.u. We observe similar phenomena for other ions also. For  $2s$  and  $2p$  states of H-like ions embedded in SCP, ‘*incidental degeneracy*’ and ‘*level crossing*’ phenomena are evident from tables 6 – 8 and being reported here for the first time.

In table 10, we have displayed the comparison of present results for transition energies of  $C^{4+}$ ,  $Al^{11+}$  and  $Ar^{16+}$  with experimental measurements [22–24] and existing theoretical calculations [36]. Table-10 clearly depicts that the present results are in good agreement with the experimental measurements as compared to other theoretical results. The difference between theoretical and experimental results is due to the relativistic effects which is more significant for  $Al^{11+}$  and  $Ar^{16+}$  than  $C^{4+}$ . For  $Ar^{16+}$  confined in ion-sphere, Sil *et al.* [36] have made a comparison of theoretically calculated transition energies with the experiments but the plasma electron density reported by them is one order less than the experimental condition of  $1.0 \times 10^{24}$  per c.c. [24] and the IS radius of 2.057 a.u. [36] also does not correspond to any of the densities. Actually, according to eq. (4), IS radius of 2.057 a.u. corresponds to a plasma electron density of  $2.96 \times 10^{24}$  per c.c. for  $Ar^{16+}$ . We have calculated the energies corresponding to  $1s^2 \rightarrow 1snp$  [ $n = 2 - 4$ ] transitions of  $Ar^{16+}$  for both experimental [24] and theoretical [36] conditions and given the values in table-10. It is seen from table-10 that the  $1s^2 \rightarrow 1s5p$  transition energies estimated from present results are more away from experiments as compared to other transitions. We note that present size of the trial wave function for a high-lying state like  $1s5p$  ( $^1P^o$ ) is not sufficient and needs to be increased to obtain greater accuracy.

The thermodynamic pressure experienced by H-like and He-like  $C$ ,  $Al$  and  $Ar$  in their respective ground states have been calculated for different values of IS radius  $R$  using eq. (22) and the results are given in table-11. It is clear from table-11 that as  $n_e$  increases, the pressure upon the ion increases and the ion moves towards destabilization. We observe that for a low value of  $n_e$ , the pressure upon the one-electron ion is higher than the respective two-electron ion and after a certain increase of  $n_e$ , the pressure on the two-electron ion exceeds the pressure experienced by the corresponding one-electron ion. With a view to studying the variation of thermodynamic pressure ( $P$ ) with respect to the IS volume ( $V$ ) under an adiabatic expansion, we have tried to fit the results for the two-electron ions obtained from the present calculations according to the ideal gas relation,

$$PV^\gamma = constant \quad \text{or} \quad \ln P + \gamma \ln V = constant \quad (30)$$

where  $\gamma$  is the ratio of two specific heats. From a least square fit of  $\ln P$  vs.  $\ln V$  plot, the value of  $\gamma$  comes out to be close to 1.4 for all the two-electron ions. To be precise, for  $C^{4+}$ ,  $Al^{11+}$  and  $Ar^{16+}$ , the values of  $\gamma$  are 1.41, 1.37 and 1.37 respectively.

## 4 Conclusion

Accurate analytical evaluation of the two-electron correlated integrals in Hylleraas coordinates within a finite limit has been performed. The intricacies of such calculations have been discussed in detail and the general applicability of these integrals has been established for arbitrary values of physically acceptable parameters. This methodology has immense potential to be useful for evaluation of the energy values and other spectral properties for three-body ionic and exotic systems placed within different external confinements such as strongly and moderately coupled plasma, fullerene cages, barrier potential, potential well *etc.* With the recent advancement in experimental technique, the present methodology becomes relevant for calculating accurate plasma electron density from the spectral analysis of hydrogen and helium-like ions. We conclude that the ion-sphere potential where the electron density is calculated by using the SP model of IPDs provides a realistic picture of ions embedded in SCP environment. The present non-relativistic results reported here can be useful for plasma diagnostics and the non-relativistic energy values can serve as benchmark for future calculations to estimate relativistic and QED effects on two-electron ions within finite domain.

## Acknowledgment

SB acknowledges financial support under grant number PSW-160/14-15(ERO) from University Grants Commission, Govt. of India. TKM acknowledges financial support under grant number 37(3)/14/27/2014-BRNS from the Department of Atomic Energy, BRNS, Govt. of India.

## References

- [1] J. Sabin and E. Brandas (*Ed.*) and prefaced by S. A. Cruz, *Adv. Quantum Chem.* **58** (2009).
- [2] P. A. Jacobs, *Carboniogenic Activity of Zeolites* (Amsterdam: Elsevier) (1997).
- [3] Y. B. Xu, M. Q. Tan, and U. Becker, *Phys. Rev. Lett.* **76**, 3538 (1996).
- [4] A.N. Sil, S. Canuto, and P. K. Mukherjee, *Adv. Quantum Chem.* **58**, 115 (2009) and references therein.
- [5] S. Canuto (*ed.*) *Solvation Effects on Molecules and Biomolecules, Computational Methods and Applications* (Berlin: Springer) (2008).
- [6] C.A. Walsh, J. Yuan, and L.M. Brown, *Philos. Mag. B* **80**, 1507 (2000).
- [7] M. Koskinen, M. Manninen, and S. M. Reimann, *Phys. Rev. Lett.* **79**, 1389 (1997).
- [8] J. Cioslowski and E. D. Fleischmann, *J. Chem. Phys.* **94**, 3730 (1991).
- [9] L. Turker, *Int. J. Hydrogen Energy* **32**, 1933 (2007).
- [10] T. Guillot, *Planet Space Sci.* **47**, 1183 (1999).
- [11] J. K. Saha, S. Bhattacharyya, and T. K. Mukherjee, *Int. Rev. At. Mol. Phys.* **3**, 1 (2012).

- [12] J. K. Saha, S. Bhattacharyya, P. K. Mukherjee, and T. K. Mukherjee, *J. Quant. Spec. Rad. Trans.* **111**, 675 (2010).
- [13] J. K. Saha, S. Bhattacharyya, P. K. Mukherjee, and T. K. Mukherjee, *J. Phys. B* **42**, 245701 (2009).
- [14] A. F. Ordonez-Lasso, J. C. Cardona, and J. L. Sanz-Vicario, *Phys. Rev. A* **88**, 012702 (2013).
- [15] L. G. Jiao and Y. K. Ho, *Phys. Rev. A* **87**, 052508 (2013).
- [16] M. Das, M. Das, R. K. Chaudhuri and S. Chattopadhyay, *Phys. Rev. E* **85**, 042506 (2012).
- [17] S. B. Zhang, J. G. Wang and R. K. Janev, *Phys. Rev. Lett.* **104**, 023203 (2010).
- [18] M. Das, R. K. Chaudhuri, S. Chattopadhyay, U. S. Mahapatra, and P. K. Mukherjee, *J. Phys. B* **44**, 165701 (2011).
- [19] J. P. Santos, A. M. Costa, J. P. Marques, M. C. Martins, P. Indelicato, and F. Parente, *Phys. Rev. A* **82**, 062516 (2010).
- [20] A. I. Akhiezer, I. A. Akhiezer, R. A. Polovin, A. G. Sitenko and K. N. Stepanov, *Plasma Electrodynamics, Linear Response Theory* (Oxford, Pergamon), Vol. 1 (1975).
- [21] S. Ichimaru, *Rev. Mod. Phys.* **54**, 1017 (1982).
- [22] M. Nantel, G. Ma, S. Gu, C.Y. Cote, J. Itatani, and D. Umstadter, *Phys. Rev. Lett.* **80**, 4442 (1998).
- [23] A. Saemann, K. Eidmann, I. E. Golovkin, R. C. Mancini, E. Andersson, E. Forster, and K. Witte, *Phys. Rev. Lett.* **82**, 4843 (1999).
- [24] N. C. Woolsey, B. A. Hammel, C. J. Keane, C. A. Back, J. C. Moreno, J. K. Nash, A. Calisti, C. Mosse, R. Stamm, B. Talin, A. Asfaw, L. S. Klein, and R. W. Lee, *Phys. Rev. E* **57**, 4650 (1998).
- [25] S. M. Vinko *et al.*, *Nature Communications* **6**, 6397 (2015).
- [26] S. M. Vinko *et al.*, *Nature* **482**, 59 (2012).
- [27] O. Ciricosta *et al.*, *Phys. Rev. Lett.* **109**, 065002 (2012).
- [28] B. I. Cho *et al.*, *Phys. Rev. Lett.* **109**, 245003 (2012).
- [29] J. C. Stewart Jr., K. D. Pyatt, *Astrophys. J.* **144**, 1203 (1966).
- [30] G. Ecker and W. Kröll, *Phys. Fluids* **6**, 62 (1963).
- [31] T. R. Preston, S. M. Vinko, O. Ciricosta, H. K. Chung, R. W. Lee, and J. S. Wark, *High Energy Density Physics* **9**, 258 (2013).
- [32] D. R. Inglis and E. Teller, *Astrophys. J.* **90**, 439 (1939).
- [33] D. J. Hoarty *et al.*, *Phys. Rev. Lett.* **110**, 265003 (2013).
- [34] D. J. Hoarty *et al.*, *High Energy Density Physics* **9**, 661 (2013).
- [35] S. K. Son, R. Thiele, Z. Jurek, B. Ziaja, and R. Santra, *Phys. Rev. X* **4**, 031004 (2014)

- [36] A. N. Sil, J. Anton, S. Fritzsche, P. K. Mukherjee, and B. Fricke, *Eur. Phys. J. D* **55**, 645 (2009) and references therein.
- [37] N. Aquino, A. Flores-Riveros, and J. F. Rivas-Silva, *Phys. Lett. A* **307**, 326 (2003).
- [38] A. Flores-Riveros, and A. Rodriguez-Contreras, *Phys. Lett. A* **372**, 6175 (2008).
- [39] C. Laughlin, and S. I. Chu, *J. Phys. A: Math. Theor.* **42**, 265004 (2009).
- [40] A. Flores-Riveros, N. Aquino, and H. E. Montgomery Jr., *Phys. Lett. A* **374**, 1246 (2010).
- [41] S. Bhattacharyya, J. K. Saha, P. K. Mukherjee, and T. K. Mukherjee, *Physica Scripta* **87**, 065305 (2013).
- [42] H. E. Montgomery Jr., and V. I. Pupyshev, *Phys. Lett. A* **377**, 2880 (2013).
- [43] K. D. Sen, *J. Chem. Phys.* **122**, 194324 (2005).
- [44] A. K. Bhatia, and A. Temkin, *Rev. Mod. Phys.* **36**, 1050 (1964).
- [45] T. K. Mukherjee, and P. K. Mukherjee, *Phys. Rev. A* **50**, 850 (1994).
- [46] J. K. Saha, S. Bhattacharyya, P. K. Mukherjee and T. K. Mukherjee, *Chem. Phys. Lett.* **517**, 223 (2011).
- [47] J. A. Nelder, and R. Mead, *Comput. J.* **7**, 308 (1965).
- [48] J. K. Saha, and T. K. Mukherjee, *Phys. Rev. A* **80**, 022513 (2009).
- [49] E. A. Carrillo-Delgado, I. Rodriguez-Vargas, and S. J. Vlaev, *PIERS Online* **5**, 137 (2009) *and references therein*.
- [50] F. Capasso, C. Sirtori, J. Faist, D. L. Sivco, S. G. Chu, and A. Y. Cho, *Nature* **358**, 565 (1992).

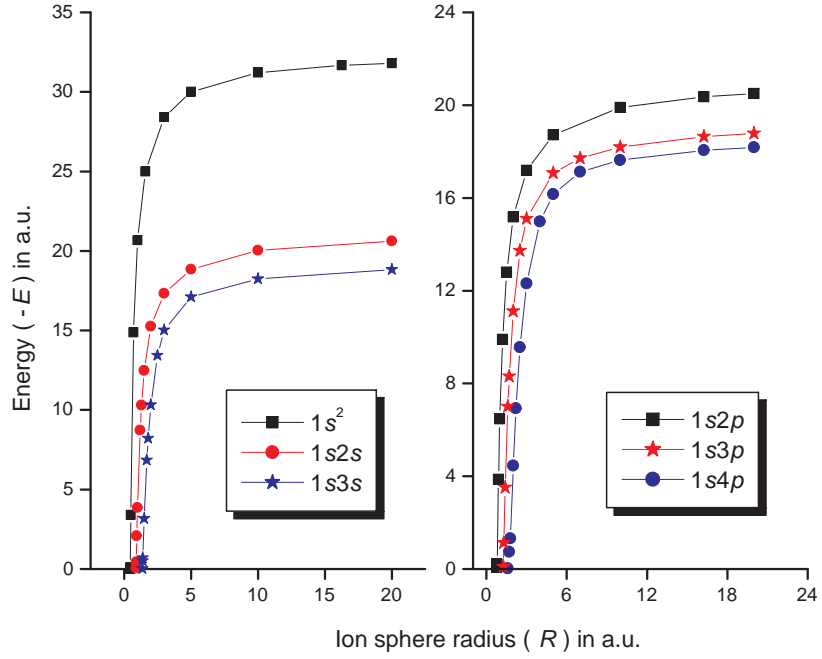


Figure 1: Variation of eigen energies  $(-E)$  of bound  $1sns(^1S^e)$  [ $n = 1-3$ ] and  $1sn'p(^1P^o)$  [ $n' = 2-4$ ] states of  $C^{4+}$  with respect to ion-sphere radius  $R$ .

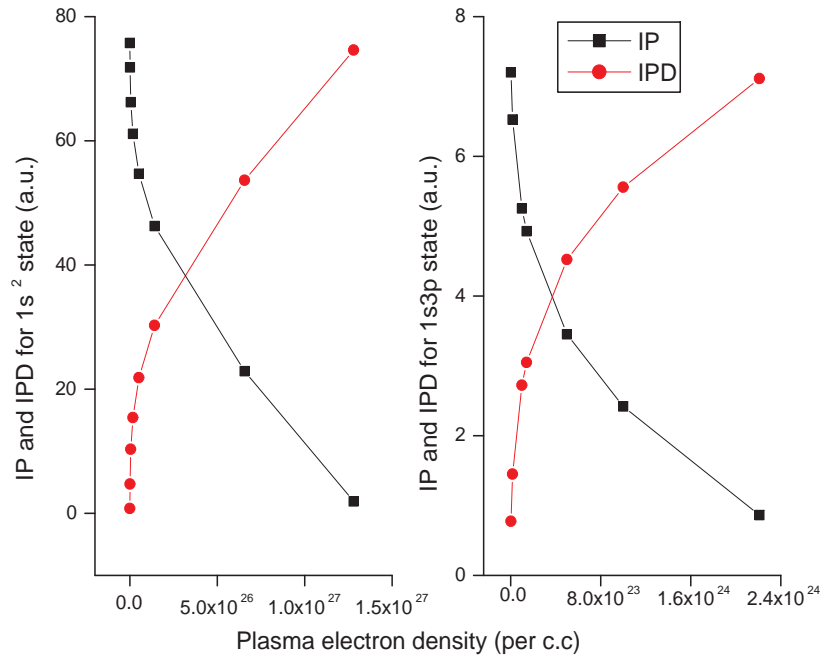


Figure 2: Variation of IP and IPD for  $1s^2$  ( $^1S^e$ ) and  $1s3p$  ( $^1P^o$ ) states of  $Al^{11+}$  with respect to plasma electron density.

Table 1: Values of integral  $A(a, b, c; \alpha, \beta; R)$  with  $a \geq 0, b \geq 0, c \geq 0$ . The notation  $x(y)$  indicates  $x \times 10^y$ .

$(a, b, c)$	$\alpha$	$\beta$	$R$	$A(a, b, c; \alpha, \beta; R)$
(0,0,0)	0.62450527	0.41287135	100.0	0.7477 2634 8987 8847 (+01)
			2.0	0.1578 7453 6391 8980 (+01)
			0.2	0.4688 3009 2327 4260 (-02)
	8.92934001	5.97270373	100.0	0.2516 4820 0437 6827 (-02)
			2.0	0.2516 4546 4241 1431 (-02)
			0.2	0.9770 3676 6565 7275 (-03)
	17.42010556	10.32300145	100.0	0.4008 8345 0596 5748 (-03)
			2.0	0.4008 8344 9906 8468 (-03)
			0.2	0.3006 0461 4922 4955 (-03)
(2,3,1)	0.62450527	0.41287135	100.0	0.1578 2446 3158 5587 (+06)
			2.0	0.9755 4412 5697 4906 (+01)
			0.2	0.4326 2415 0573 9082 (-07)
	8.92934001	5.97270373	100.0	0.5960 1910 9088 6659 (-05)
			2.0	0.5913 0152 3072 3085 (-05)
			0.2	0.4824 7810 4677 3954 (-08)
	17.42010556	10.32300145	100.0	0.2667 8377 6884 8479 (-07)
			2.0	0.2667 8110 4519 4153 (-07)
			0.2	0.7198 6505 5902 0197 (-09)
(3,4,6)	0.62450527	0.41287135	100.0	0.5959 0474 3300 4562 (+14)
			2.0	0.3133 2861 0504 5369 (+04)
			0.2	0.1612 2935 4296 9925 (-11)
	8.92934001	5.97270373	100.0	0.1741 4651 3311 5703 (-04)
			2.0	0.1311 5563 4874 3337 (-04)
			0.2	0.1427 2637 0766 0009 (-12)
	17.42010556	10.32300145	100.0	0.1312 3966 9657 3856 (-08)
			2.0	0.1305 9386 1401 5103 (-08)
			0.2	0.1601 5416 4752 0373 (-13)

Table 2: Values of integral  $I(\alpha, \beta; R)$ . Results obtained by using eq. (28) and eq. (29) are given in consecutive rows respectively. The notation  $x(y)$  indicates  $x \times 10^y$ .

$\alpha$	$\beta$	$R$	$I(\alpha, \beta; R)$			
0.62450527	0.41287135	100.0	0.2910 1096 5167 7626 (+9)			
				0.5074 9055 6270 2974		
			2.0	0.4049 6455 3461 7721		
		8.92934001	5.97270373	100.0	0.4049 6455 3461 7721	
					0.2	0.0760 8455 8526 4357
						0.0760 8455 8526 4357
		17.42010556	10.32300145	100.0	0.2617 9165 1879 3351 (+602)	
					2.0	0.5121 5588 2201 4390
						0.5121 5588 1268 8812
		0.2	0.5121 5588 1268 8812			
				0.4595 0838 7239 3843		
				0.4595 0838 7239 3843		
		100.0	0.9419 3093 2537 1151 (+872)			
			2.0	0.4653 6238 2193 5131		
				0.4653 6238 2193 5052		
		0.2	0.4653 6238 2193 5131			
				0.4588 5876 8812 0597		
				0.4588 5876 8812 0597		

Table 3: Convergence of the integral  $I(\alpha, \beta; R)$  *w.r.t.* the number of terms ( $q$ ) in the infinite series using equations (28) and (29). The notation  $x(y)$  indicates  $x \times 10^y$ .

$\alpha$	$\beta$	$R$	$q$	$I(\alpha, \beta; R)$			
				Eq. (28)	Eq. (29)		
0.62450527	0.41287135	100	10	-0.3568 5265 8756 6828 (+13)	0.5068 9300 3143 0272		
			20	-0.3554 0371 2221 5343 (+21)	0.5074 8564 3805 4664		
			50	-0.2755 0482 1577 0421 (+35)	0.5074 9055 6262 6217		
			100	-0.2124 7555 4344 8736 (+42)	0.5074 9055 6270 2974		
			1000	0.2910 1096 5167 7626 (+09)	0.5074 9055 6270 2974		
		0.2	10	0.0760 8455 8526 4356	0.0760 8455 8526 4357		
			20	0.0760 8455 8526 4357	0.0760 8455 8526 4357		
			50	0.0760 8455 8526 4357	0.0760 8455 8526 4357		
			100	0.0760 8455 8526 4357	0.0760 8455 8526 4357		
			1000	0.0760 8455 8526 4357	0.0760 8455 8526 4357		
		17.42010556	10.32300145	100	10	-0.7343 5142 7504 1944 (+27)	0.4651 7579 3447 4452
					20	-0.1488 0713 2757 9564 (+50)	0.4653 6186 8073 0945
					50	-0.9285 2359 3991 9110 (+106)	0.4653 6238 2193 4812
					100	-0.2137 8120 9553 6411 (+185)	0.4653 6238 2193 5131
1000	-0.2609 9042 7983 5017 (+873)				0.4653 6238 2193 5131		
0.2	10			0.2166 5736 2229 1603	0.4588 5852 3846 0869		
	20			0.4588 5558 5227 7264	0.4588 5876 8812 0596		
	50			0.4588 5876 8812 0597	0.4588 5876 8812 0597		
	100			0.4588 5876 8812 0597	0.4588 5876 8812 0597		
	1000			0.4588 5876 8812 0597	0.4588 5876 8812 0597		

Table 4: Values of integral  $A(a, b, c; \alpha, \beta; R)$  with  $a = -1, b \geq 0, c \geq 0$ . The notation  $x(y)$  indicates  $x \times 10^y$ .

$(a, b, c)$	$\alpha$	$\beta$	$R$	$A(-1, b, c; \alpha, \beta; R)$
(-1,0,0)	0.62450527	0.41287135	100.0	0.5954 2692 0365 7702 (+01)
			2.0	0.2328 7535 9564 1012 (+01)
			0.2	0.5410 3409 5795 4025 (-01)
	8.92934001	5.97270373	100.0	0.2871 3769 8867 2015 (-01)
			2.0	0.2871 3526 4943 5828 (-01)
			0.2	0.1630 9271 2387 9263 (-01)
	17.42010556	10.32300145	100.0	0.8733 9216 7581 8471 (-02)
			2.0	0.8733 9216 6380 3946 (-02)
			0.2	0.7244 1513 1903 8541 (-02)
(-1,3,0)	0.62450527	0.41287135	100.0	0.6567 2317 0086 4201 (+03)
			2.0	0.4615 4100 9066 9881 (+01)
			0.2	0.1352 9814 0488 3989 (-03)
	8.92934001	5.97270373	100.0	0.1048 5277 9488 0441 (-02)
			2.0	0.1046 0034 4655 7635 (-02)
			0.2	0.2845 3033 4471 0229 (-04)
	17.42010556	10.32300145	100.0	0.6034 8938 8061 1726 (-04)
			2.0	0.6034 8827 2996 3596 (-04)
			0.2	0.8940 2524 7131 8926 (-05)
(-1,6,4)	0.62450527	0.41287135	100.0	0.1994 0115 8159 1710 (+12)
			2.0	0.3251 2782 4902 2441 (+03)
			0.2	0.1201 4454 0849 6434 (-08)
	8.92934001	5.97270373	100.0	0.2402 8418 0970 4088 (-02)
			2.0	0.1563 9297 5468 9225 (-02)
			0.2	0.1788 1043 5252 0599 (-09)
	17.42010556	10.32300145	100.0	0.2982 9940 1992 8102 (-05)
			2.0	0.2960 5934 0875 9482 (-05)
			0.2	0.4140 7243 9026 4580 (-10)

Table 5: Convergence of energy values ( $-E$  a.u.) of  $1s^2(^1S^e)$  state of  $C^{4+}$  with respect to number of terms ( $N$ ) in wave function within Ion-sphere radius  $R$  a.u.

State	$N$	$-E$ for two-electron ions				
		$R = 20.0$	0.7	0.5	0.47	0.4692
$1s^2(^1S^e)$	13	31.8060 7622	14.8798 5637	3.4091 6161	0.1035 1773	0.0053 4000
	22	31.8062 6559	14.8805 9032	3.4092 5286	0.1037 0540	0.0055 3914
	34	31.8062 9082	14.8806 1939	3.4092 6383	0.1037 1810	0.0055 5223
	50	31.8062 9351	14.8806 2562	3.4092 6610	0.1037 1980	0.0055 5423
	70	31.8062 9412	14.8806 2707	3.4092 6664	0.1037 2017	0.0055 5462
	95	31.8062 9431	14.8806 2746	3.4092 6678	0.1037 2026	0.0055 5471
	125	31.8062 9439	14.8806 2759	3.4092 6682	0.1037 2029	0.0055 5474
	161	31.8062 9443	14.8806 2763	3.4092 6683	0.1037 2029	0.0055 5475

Table 6: Energy eigenvalues ( $-E$  a.u.) of  $C^{4+}$  and  $C^{5+}$  within ion-sphere of Radius  $R$  a.u. Densities (per c.c.) are determined from radius by using eq. (4). The uncertainty of the calculated energy values is of the order of  $10^{-6}$  a.u.

Plasma		$-E$ for two-electron ions						$-E$ for one-electron ions				
density	R	$1s^2$	$1s2s$	$1s3s$	$1s2p$	$1s3p$	$1s4p$	R	$E_{1s}$	$E_{2s}$	$E_{2p}$	$E_{3p}$
	$C^{4+}$							$C^{5+}$				
8.05(20)	20.0	31.806 294	20.622 433	18.819 815	20.493 660	18.782 365	18.183 990	21.544	17.651 901	4.152 167	4.151 006	1.298 528
1.50(21)	16.256	31.668 147			20.355 753	18.645 771	18.051 134	17.511	17.571 741	4.072 241	4.070 983	1.216 051
6.44(21)	10.0	31.206 629	20.025 353	18.234 022	19.895 956	18.195 421	17.626 905	10.772	17.303 930	3.806 085	3.804 210	0.941 359
1.88(22)	7.0					17.710 079	17.127 014	7.540	17.005 859	3.512 120	3.508 790	0.638 130
5.15(22)	5.0	30.009 311	18.848 891	17.115 098	18.714 486	17.073 177	16.164 573	5.386	16.608 855	3.126 251	3.119 111	0.239 771
8.32(22)								4.591			2.885 861	0.001 097
1.01(23)	4.0						14.979 005	4.309	16.262 009	2.796 224	2.783 284	
2.39(23)	3.0	28.420 442	17.332 928	15.017 054	17.183 256	15.108 681	12.307 491	3.232	15.685 381	2.266 340	2.237 178	
4.12(23)	2.5			13.431 934		13.720 854	9.562 152	2.693	15.225 721	1.855 508	1.812 626	
6.05(23)	2.2						6.922 023	2.370	14.850 960	1.512 931	1.468 923	
8.05(23)	2.0		15.256 681	10.320 034	15.180 308	11.114 072	4.454 707	2.154	14.539 678	1.207 836	1.175 386	
1.10(24)	1.8			8.209 279			1.315 545	1.939	14.160 665	0.797 941	0.799 140	
1.31(24)	1.7			6.840 488		8.309 520	0.736 221	1.831	13.938 515	0.529 722	0.563 106	
1.57(24)	1.6	24.999 764				7.004 681		1.723	13.689 353	0.200 592	0.283 113	
1.58(24)	1.596						0.030 797	1.719	13.678 753	0.186 970	0.271 734	
1.85(24)								1.632			0.003 072	
1.91(24)	1.5		12.478 314	3.173 818	12.790 730			1.616	13.407 990			
2.35(24)	1.4			0.691 166		3.506 751		1.508	13.087 774			
2.38(24)	1.3937			0.516 288				1.501	13.066 138			
2.47(24)	1.3761			0.015 255				1.482	13.004 619			
2.93(24)	1.3		10.292 255			1.124 349		1.400	12.720 153			
3.20(24)	1.263					0.096 911		1.360	12.569 908			
3.73(24)	1.2		8.722 057		9.902 622			1.293	12.293 555			
6.44(24)	1.0	20.674 940	3.865 288		6.473 522			1.077	11.190 638			
7.52(24)	0.95		2.091 381					1.023	10.841 350			
8.55(24)	0.91		0.434 054					0.980	10.532 355			
8.79(24)	0.9017		0.059 416					0.971	10.464 484			
8.84(24)	0.9				3.864 058			0.969	10.450 413			
1.25(25)	0.8				0.209 360			0.862	9.499 773			
1.27(25)	0.797				0.077 557			0.858	9.466 811			
1.88(25)	0.7	14.880 628						0.754	8.198 121			
5.15(25)	0.5	3.409 267						0.539	2.956 871			
6.21(25)	0.47	0.103 720						0.5063	1.497 759			
6.23(25)	0.4695	0.042 434						0.5057	1.470 782			
6.24(25)	0.4692	0.005 555						0.5054	1.454 571			

Table 7: Energy eigenvalues ( $-E$  a.u.) of  $Al^{11+}$  and  $Al^{12+}$  within ion-sphere of Radius  $R$  a.u. Densities (per c.c.) are determined from radius by using eq. (4). The uncertainty of the calculated energy values is of the order of  $10^{-6}$  a.u.

Plasma density	$-E$ for two-electron ions							$-E$ for one-electron ions				
	R	$1s^2$	$1s2s$	$1s3s$	$1s2p$	$1s3p$	$1s4p$	R	$E_{1s}$	$E_{2s}$	$E_{2p}$	$E_{3p}$
	$Al^{11+}$							$Al^{12+}$				
2.21(21)	20.0	159.382 029	101.075 286	90.920 760	100.751 849	90.826 863	87.343 470	20.589	83.625 742	20.250 901	20.250 869	8.508 494
1.77(22)	10.0	157.732 211	99.426 741	89.277 651	99.102 949	89.183 005	85.713 789	10.294	82.751 557	19.377 826	19.377 385	7.638 134
5.17(22)	7.0	156.318 323	98.015 642	87.878 476				7.206	82.002 366	18.631 067	18.629 929	6.898 570
1.00(23)	5.617	155.158 153			96.533 764	86.640 729	83.249 437	5.782	81.387 603	18.019 768	18.017 402	6.297 680
1.42(23)	5.0				95.811 753	85.932 485	82.582 105	5.147	81.003 693	17.638 853	17.635 633	5.926 068
5.00(23)	3.285	150.992 205			92.391 567	82.632 916	79.441 867	3.382	79.179 940	15.840 819	15.830 292	4.207 565
6.56(23)	3.0	150.039 702	91.786 850	81.867 981				3.088	78.675 129	15.347 266	15.332 246	3.746 670
1.00(24)	2.607	148.385 508			89.814 745	80.216 318		2.684	77.798 403	14.495 335	14.473 891	2.966 481
2.21(24)	2.0	144.557 994	86.435 075	76.751 134	86.060 502	76.632 056	70.991 150	2.058	75.769 505	12.554 606	12.501 889	1.209 389
3.31(24)								1.8			11.309 886	0.084 801
5.25(24)	1.5	139.093 636	81.216 562	70.476 891	80.776 714	70.672 695	59.958 894	1.544	72.871 972	9.877 422	9.760 672	
1.77(25)	1.0	128.240 365	70.674 599	51.222 379	70.269 488	53.774 530	27.642 101	1.029	67.112 431	4.647 358	4.445 998	
2.43(25)	0.9				66.602 776		13.910 306	0.926	65.206 039	2.699 333	2.596 821	
3.10(25)	0.83			34.498 851	63.390 834		1.358 983	0.854	63.604 555	0.880 652	0.952 002	
3.21(25)	0.82						0.585 110	0.844	63.354 014	0.578 268	0.692 836	
3.31(25)	0.812						0.088 777	0.836	63.149 234	0.327 244	0.479 227	
3.46(25)	0.8		61.584 852	30.304 265				0.823	62.834 616		0.011 954	
5.17(25)	0.7	114.496 531	54.024 877	11.937 344	55.190 310	21.877 996		0.721	59.806 678			
5.64(25)	0.68			7.201 566				0.700	59.097 854			
6.16(25)	0.66			2.007 102				0.6794	58.347 614			
6.18(25)	0.6594			1.843 590				0.6788	58.324 454			
6.37(25)	0.65283			0.022 248				0.672	58.067 871			
6.45(25)	0.65						11.929 838	0.669	57.955 830			
7.81(25)	0.61						2.170 876	0.628	56.265 059			
8.08(25)	0.603						0.262 866	0.621	55.946 962			
8.10(25)	0.6025						0.124 062	0.6202	55.923 954			
8.11(25)	0.6021						0.012 689	0.6198	55.905 567			
1.41(26)	0.5	96.523 118	22.189 554		30.281 348			0.515	50.268 732			
2.08(26)	0.44		2.370 513					0.453	45.729 585			
2.14(26)	0.436		0.724 569					0.449	45.379 873			
2.15(26)	0.4351		0.347 428					0.448	45.300 161			
2.16(26)	0.43434		0.026 971					0.447	45.232 635			
2.77(26)	0.4				3.174 966			0.412	41.877 044			
2.87(26)	0.395				1.274 781			0.407	41.331 971			
2.95(26)	0.3918				0.020 739			0.403	40.974 430			
6.56(26)	0.3	49.123 982						0.309	26.244 361			
1.28(27)	0.24	8.502 491						0.247	6.577 159			
1.419(27)	0.232	0.362 136						0.239	2.673 160			
1.424(27)	0.2317	0.038 819						0.238	2.518 185			

Table 8: Energy eigenvalues ( $-E$  a.u.) of  $Ar^{16+}$  and  $Ar^{17+}$  within ion-sphere of Radius  $R$  a.u. Densities (per c.c.) are determined from radius by using eq. (4). The uncertainty of the calculated energy values is of the order of  $10^{-6}$  a.u.

Plasma density	$-E$ for two-electron ions							$-E$ for one-electron ions				
	R	$1s^2$	$1s2s$	$1s3s$	$1s2p$	$1s3p$	$1s4p$	R	$E_{1s}$	$E_{2s}$	$E_{2p}$	$E_{3p}$
	$Ar^{16+}$							$Ar^{17+}$				
3.22(21)	20.0	310.507 205	196.041 306	175.755 299	195.578 034	175.620 951	168.619 605	20.408	160.750 518	39.250 638	39.250 583	16.751 038
2.58(22)	10.0	308.107 341	193.642 370	173.360 319	193.178 832	173.225 396	166.234 270	10.204	159.501 078	38.002 041	38.001 721	15.505 423
2.06(23)	5.0	303.308 425	188.850 886	168.600 563	188.385 210	168.461 043	161.553 149	5.102	157.002 621	35.510 327	35.507 887	13.037 578
9.55(23)	3.0						155.654 881	3.061	153.672 785	32.208 489	32.196 858	9.835 118
2.11(24)	2.3						151.183 198	2.347	151.140 923	29.720 258		
2.96(24)	2.057	289.590 037			174.748 078	155.284 420	148.653 416	2.099	149.859 811	28.470 821	28.436 728	6.367 203
3.22(24)	2.0	288.926 557	174.593 816	154.885 258	174.092 315	154.670 904	147.924 331	2.041	149.514 344	28.135 153	28.099 008	6.066 598
7.64(24)	1.5			147.515 430			147.294 212	1.531	145.362 038	24.149 851	24.065 320	2.548 088
1.22(25)								1.309			21.374 828	0.027 313
1.49(25)	1.2			139.209 711			123.092 431	1.224	141.218 060	20.283 441	20.102 175	
2.58(25)	1.0	265.062 279	151.634 784	129.063 495	150.887 572	129.848 525	105.387 057	1.020	137.084 181	16.548 570	16.250 296	
5.03(25)	0.8			109.499 582			72.434 154	0.816	130.907 580	11.023 329	10.593 320	
7.51(25)	0.7	244.788 710	140.318 457	92.135 024	131.230 710	97.682 171	44.281 500	0.714	126.516 643	6.834 684	6.481 745	
9.39(25)	0.65						25.066 379	0.663	123.824 592	4.030 093	3.846 749	
1.13(26)	0.61						6.173 887	0.622	121.360 487	1.249 801	1.311 525	
1.18(26)	0.6014						1.639 257	0.614	120.788 926	0.571 762	0.762 695	
1.19(26)	0.6			64.536 211				0.612	120.694 413	0.458 366	0.622 378	
1.201(26)	0.5987						0.228 118	0.6109	120.606 199	0.352 195	0.544 660	
1.203(26)	0.59843						0.067 636	0.6106	120.587 871	0.330 097	0.523 396	
1.24(26)								0.604			0.048 119	
2.06(26)	0.5	218.150 195	99.801 076	17.342 729	102.188 104	37.003 115		0.510	112.615 414			
2.19(26)	0.49			10.878 182				0.500	111.632 327			
2.33(26)	0.48			3.985 508				0.4898	110.609 857			
2.344(26)	0.4791			3.342 920				0.4889	110.515 854			
2.345(26)	0.47902			3.285 614				0.4888	110.507 440			
2.41(26)	0.47455			0.035 558				0.4842	110.035 148			
2.83(26)	0.45						8.128 548	0.4592	107.280 138			
3.053(26)	0.4387						0.218 634	0.448	105.912 248			
3.059(26)	0.43843						0.022 169	0.447	105.878 796			
4.03(26)	0.4		63.058 578		72.434 796			0.408	100.662 918			
6.01(26)	0.35		30.887 328					0.357	92.198 308			
7.87(26)	0.32		3.274 140					0.326	85.821 161			
8.01(26)	0.318		1.126 899					0.3245	85.350 316			
8.04(26)	0.3176		0.692 178					0.3241	85.255 417			
8.05(26)	0.31751		0.594 121					0.3240	85.233 983			
8.09(26)	0.31698		0.014 841					0.323	85.107 902			
9.55(26)	0.3	156.809 245						0.306	80.799 235			
1.08(27)	0.288				0.703 578			0.294	77.402 624			
1.09(27)	0.2874				0.09 253			0.293	77.224 113			
3.22(27)	0.2	64.368 049						0.204	34.699 257			
4.42(27)	0.18	25.307 474						0.184	15.611 535			
5.15(27)	0.171	2.741 398						0.1745	4.631 691			
5.24(27)	0.1701	0.269 467						0.1736	3.429 550			
5.25(27)	0.17001	0.019 935						0.1735	3.308 080			

Table 9: Critical plasma electron densities after which spectral lines of hydrogen-like and helium-like  $Al$  disappear. Densities are obtained from IS radii according to both SP model [eq. (4)] and EK model[eq. (5)] for IPDs. The notation  $x(y)$  indicates  $x \times 10^y$ .

Z	Spectral line	Critical plasma electron density (per c.c.)			
		Present results		Other results	
		SP model <sup>a</sup>	EK model <sup>b</sup>	Experiment	Theory
6	$Ly_\alpha$	1.85(24)	1.19(24)		
	$Ly_\beta$	8.32(22)	2.77(22)		
	$He_\alpha$	8.05(23)	1.61(23)		
	$He_\beta$	5.15(22)	1.03(22)		
	$He_\gamma$	1.88(22)	3.76(21)		
13	$Ly_\alpha$	3.52(25)	2.71(24)		
	$Ly_\beta$	3.31(24)	2.55(23)	2.2(24) <sup>c</sup>	2.93(24) <sup>d</sup> 2.64(24) – 3.3(24) <sup>e</sup>
	$He_\alpha$	2.43(25)	2.53(24)		
	$He_\beta$	2.21(24)	1.84(23)	2.2(24) <sup>c</sup>	2.44(24) <sup>d</sup> 1.98(24) – 2.64(24) <sup>e</sup>
	$He_\gamma$	5.00(23)	4.16(22)		6.60(22) – 1.32(23) <sup>e</sup>
18	$Ly_\alpha$	1.24(26)	6.90(25)		
	$Ly_\beta$	1.22(25)	6.78(23)		
	$He_\alpha$	7.51(25)	4.42(25)		
	$He_\beta$	7.64(24)	4.49(23)		
	$He_\gamma$	2.11(24)	1.25(23)		

a: Ref. [29]; b: Ref. [30]; c: Ref. [33]; d: Ref. [35]; e: Ref. [31].

Table 10: Transition energies (in Å) in strongly coupled plasma environment. Densities are calculated according eq. (4). Conversion factors :  $(\Delta E)_\text{Å} = 12395/(\Delta E)_{eV}$  and 1 *a.u.* of energy = 27.21138 *eV*. The notation  $x(y)$  indicates  $x \times 10^y$ .

Ion	Ion-sphere radius (a.u)	Plasma density (per c.c.)	Transition scheme	Present results	Experimental results	Other theory <sup>d</sup>	
						Non-rel.	Rel.
$C^{4+}$	16.256	1.5(21)	$1s^2 \rightarrow 1s2p$	40.266	40.268 <sup>a</sup>	40.208	40.700
			$\rightarrow 1s3p$	34.979	34.998 <sup>a</sup>	34.953	35.325
			$\rightarrow 1s4p$	33.451	33.469 <sup>a</sup>	33.431	33.773
			$\rightarrow 1s5p$	32.820	32.773 <sup>a</sup>	32.800	33.133
$Al^{11+}$	2.607	1.0(24)	$1s^2 \rightarrow 1s2p$	7.777	7.75 <sup>b</sup>	7.778	7.774
			$\rightarrow 1s3p$	6.682		6.684	6.682
	3.285	5.0(23)	$1s^2 \rightarrow 1s2p$	7.773		7.773	7.770
			$\rightarrow 1s3p$	6.663		6.664	6.661
			$\rightarrow 1s4p$	6.366			6.385
	5.617	1.0(23)	$1s^2 \rightarrow 1s2p$	7.770		7.769	7.767
			$\rightarrow 1s3p$	6.648	6.63 <sup>b</sup>	6.648	6.646
			$\rightarrow 1s4p$	6.334	6.31 <sup>b</sup>	6.334	6.332
			$\rightarrow 1s5p$	6.211	6.17 <sup>b</sup>	6.205	6.212
	$Ar^{16+}$	3.856	4.5(23)	$1s^2 \rightarrow 1s2p$	3.379	3.363 <sup>c</sup>	
3.119		8.5(23)	$1s^2 \rightarrow 1s2p$	3.3811	3.364 <sup>c</sup>		
3.061		9.0(23)	$1s^2 \rightarrow 1s2p$	3.3813	3.365 <sup>c</sup>		
2.955		1.0(24)	$1s^2 \rightarrow 1s2p$	3.964	3.984 <sup>c</sup>		
			$\rightarrow 1s3p$	3.382	3.365 <sup>c</sup>		
			$\rightarrow 1s4p$	3.225	3.168 <sup>c</sup>		
2.057		2.96(24)	$1s^2 \rightarrow 1s2p$	3.966		3.964	3.950
			$\rightarrow 1s3p$	3.392		3.382	3.370
	$\rightarrow 1s4p$		3.232		3.226	3.215	

a: Ref. [22]; b: Ref. [23]; c: Ref. [24]; d: Ref. [36]

Table 11: Thermodynamic pressure on the ground state of one and two-electron ions within ion-sphere. Conversion factor : 1 a.u. of pressure = 2.9421912(13) Pa. The notation  $x(y)$  indicates  $x \times 10^y$ .

Plasma	Pressure (Pa)		Plasma	Pressure (Pa)		Plasma	Pressure (Pa)	
density	$C^{4+}$	$C^{5+}$	density	$Al^{11+}$	$Al^{12+}$	density	$Ar^{16+}$	$Ar^{17+}$
8.05(20)	0.1755(09)	0.8778(09)	2.21(21)	0.4829(09)	0.2414(10)	3.22(21)	0.7024(09)	0.3512(10)
6.44(21)	0.2807(10)	0.7019(10)	1.77(22)	0.7725(10)	0.1931(11)	2.58(22)	0.1123(11)	0.2809(11)
5.15(22)	0.4478(11)	0.5603(11)	5.17(22)	0.3217(11)	0.5630(11)	2.06(23)	0.1797(12)	0.2247(12)
2.39(23)	0.3432(12)	0.2581(12)	2.21(24)	0.4806(13)	0.2406(13)	3.22(24)	0.7007(13)	0.3504(13)
1.57(24)	0.4130(13)	0.1666(13)	1.77(25)	0.7580(14)	0.1899(14)	2.58(25)	0.1113(15)	0.2785(14)
6.44(24)	0.2779(14)	0.6681(13)	5.17(25)	0.3095(15)	0.5438(14)	2.06(26)	0.1729(16)	0.2818(15)
1.88(25)	0.1540(15)	0.1794(14)	1.41(26)	0.1178(16)	0.8791(14)	3.22(27)	0.9657(17)	0.3184(16)
5.15(25)	0.9278(15)	0.1772(14)	6.56(26)	0.1228(17)	0.1022(16)	4.42(27)	0.1667(18)	0.4212(16)
6.21(25)	0.1297(16)	0.9241(14)	1.28(27)	0.3912(17)	0.1489(16)	5.15(27)	0.2180(18)	0.8701(16)
6.23(25)	0.1304(16)	0.1123(15)	1.419(27)	0.4678(17)	0.2453(16)	5.24(27)	0.2241(18)	0.8897(16)
6.24(25)	0.1309(16)	0.1164(15)	1.424(27)	0.4710(17)	0.2466(16)	5.25(27)	0.2248(18)	0.8916(16)